Polychromatic-Microdiffraction Studies of Inhomogeneous Deformation

Gene E. Ice, Judy W.L. Pang, and Rozaliya A. Barabash

Materials Science and Technology Division, Oak Ridge National Laboratory, Oak Ridge TN 37831-6118

Abstract
Polychromatic microdiffraction is an emerging *nondestructive* probe of local crystal structure that provides *submicron-resolved* three-dimensional (3D) maps of the local phase, crystalline orientation, and the local elastic-stress and dislocation tensors. The unique ability to characterize these critical materials properties before, during, and after deformation, provides new insights and guidance for theories that attempt to include realistic local properties to model materials evolution and inhomogeneous deformation. The recent installation of dedicated polychromatic microdiffraction beamlines on powerful synchrotron sources has enabled demonstration measurements and early experiments illustrate the promise of polychromatic microdiffraction to bridge the experimental gap between atomistic and continuum scales. New instrumentation will improve spatial resolution and accelerate data collection by two to four orders of magnitude. This will allow the technique to become routinely three-dimensional and will greatly extending insights into the roles that local structures and defect distributions play in inhomogeneous deformation.

Introduction:
Inhomogeneous deformation is a ubiquitous property of materials that arises both from macroscopic and microscopic inhomogeneity and from the self-organization of defects in materials. Deformation can be either elastic (reversible on the removal of stress) or plastic (irreversible). At the macroscopic level, inhomogeneous elastic and plastic deformation is familiar; things bend or stretch most where they are narrowest or where the stress is concentrated.

At the mesoscale (~10 nm-10 μm) however, deformation physics is still an area of active research and much is still a mystery- in large part because there are few experimental tools that can nondestructively provide quantitative information on the local structure and how it evolves in 3D during deformation. Although finite-element calculations can model *aspects* of deformation in increasing complex heterogeneous samples, the essential local nature of materials behavior *can only be captured* by detailed models, that include local microstructure *and* length-scale-dependent materials physics.[1] Indeed most materials are polycrystalline- possibly multiphase-with misorientations between grains leading to *modelable local inhomogeneities*, but with grain boundary networks that impose novel and as yet unknown local properties in the grain boundary regions. Furthermore, inside single crystals and grains, dislocations organize spontaneously into networks *during deformation*.[1, 2] Both the grain boundary/ interface behavior of materials and the self-organization of defects into mesoscale structures are behaviors for which theoretical approaches are still emerging. These behaviors are critical because materials plasticity is in large part determined by mesoscale structure/defect interactions.[2]

In order to make progress in the area of deformation it is essential to test theoretical models against experiments that include the critical structures and boundary conditions and which can follow the deformation process to clarify how structures are affected by and effect local materials behavior. With this understanding, there are three essential and interrelated tensor-property distributions that must be mapped: (1) the crystal orientation tensor U^B_{ij} which describes the local elastic/plastic anisotropy; (2) the elastic strain tensor, ε_{ij}, which measures how elastic forces are accommodated by the local environment and provides a key mechanism for mesoscale dynamics; and (3) the dislocation or Nye tensor, α_{ij}, which is a fundamental input for length-scale-sensitive crystal plasticity models.[3] These tensors are interrelated, but are essential to test emerging theories of local crystal plasticity. For example, it is understood that the local elastic response in a single grain is determined predominantly by the average crystal structure, the crystal orientation and the applied stress tensor. Stress, a key driving force for mesoscale evolution can therefore be determined locally through the single crystal compliance matrix and the elastic strain tensor. In the small distortion approximation, the elastic stress/strain relationship for a single crystal is given by[4],

$$\varepsilon_{ij} = S_{ijkl}\sigma_{kl} \quad . \tag{1}$$

Here ε_{ij} is the second rank elastic strain tensor, S_{ijkl} is the fourth ranked single-crystal compliance tensor and σ_{kl} is the second ranked stress tensor. Crystal orientation and phase, which together determine the local compliance matrix, and local measurements of elastic strain, are therefore essential to determine the local stress/strain relationship.

Plastic deformation is similarly dependent on crystallographic orientation and the local stress tensor; various slip systems are activated depending on grain orientation and applied load.[5] This leads to- for example- the anisotropic rotation of grains in polycrystalline materials depending on their orientation and the applied load.[6-8] However, with *plastic* deformation, *defects and evolving mesoscale structures play a critical role* in the mechanical response to stress. It is recognized for example that dislocation walls and other features can present important barriers to dislocation motions.[2]

Recent attempts to include length scales into models of deformation have identified the key role of the dislocation tensor, α_{ij}. We adopt the dislocation tensor description used by Larson et al.[10] where,

$$\alpha_{ij} = \kappa_{ji} - (\kappa_{11} + \kappa_{22} + \kappa_{33})I_{ij} - e_{ijk}\partial_k\varepsilon_{jk} \tag{2}$$

Here κ_{ij} is the curvature tensor, I is the identity matrix and e_{ijk} is the Levi-Cevita permutation matrix. From equation 2 it is clear that careful measurements of the dislocation tensor require measurements of both the elastic strain tensor, ε_{ij} , and the curvature tensor, κ_{ij} . In fact, Larson et al. point out that whereas cases of pure elastic deformation can be achieved, cases of pure plastic deformation are more difficult to find.[10] From an experimental perspective, Eq. 2 can be understood from the recognition

that elastic strain *gradients* rotate lattice planes and smear Bragg reflections in very much the same way as do unpaired dislocations.

Polychromatic microdiffraction can nondestructively map the crystal orientation tensor and hence the compliance tensor S_{ijkl} , the elastic strain tensor σ_{kl} and the dislocation tensor α_{ij} in three dimensions. This unprecedented capability is just now being applied to resolve the behavior of local inhomogeneous deformation. This new information, together with emerging multiscale theories of deformation, experimental focused-ion-beam-milled electron backscattering diffraction and emerging x-ray high-energy imaging methods[11] is certain to revolutionize our understanding of deformation and other materials behavior. Here we introduce the techniques used in polychromatic microdiffraction and illustrate the potential of polychromatic microdiffraction with the results of recent experiments. We also identify existing resources for experiments and indicate future advances that will continue to extend capabilities.

Polychromatic Microdiffraction with Differential Aperture Microscopy

The diffraction of x-rays from crystals was first proposed by Max Von Laue[12], to verify their regular internal spacing, Laue correctly conjectured that crystals had 3D repeat spacing that acts like a natural (3D) diffraction grating for X-rays. This first diffraction application of X-rays resulted in the 1914 Nobel Prize for Physics and a comment from Einstein that the resulting Laue diffraction was one of the most beautiful discoveries in physics. Modern Laue images continue to provide beautiful pictures as evidenced by examples in this article. Subsequent research by the Braggs demonstrated that Laue diffraction is made possible by the polychromatic beams produced by x-ray sources, and that x-rays reflect off the mirror-like crystal planes when the scattering amplitudes from parallel crystal planes add constructively and hence satisfy Bragg's law.[13]

Laue diffraction is now understood in terms of the three-dimensional conditions for satisfying Bragg's law, which are graphically represented by an Ewald's sphere construction (Fig. 1). [13] In the Ewald's sphere diagram, the conditions for Bragg's law are satisfied if the momentum transfer of scattering passes through a reciprocal-space Bragg point. Reciprocal space has units of inverse distance and the possible values of momentum transfer- for a given wavelength- lie on a sphere of radius, $1/\lambda$ centered on the inverse incident beam vector (Fig. 1). The reciprocal space pattern is determined by the geometrical structure and spacing of atoms in the crystal and rotates with the crystal real-space structure.

The Ewald picture of Laue diffraction illustrates several important points: (1) wavelengths that satisfy a Bragg condition change with crystal orientation and from reciprocal space point to reciprocal space point; (2) short wavelength x-rays are more likely to intersect a reciprocal space point; and (3) Laue images are actually weighted averages of line integrals through reciprocal space.

In the modern implementation of polychromatic microdiffraction- or micro-Laue diffraction- achromatic focusing optics are used to condense an intense synchrotron x-ray

beam to a submicron spot with a depth of field of 100's of microns.[14] The beam is directed onto a sample and x-rays are diffracted into a detector mounted perpendicular to the beam axis. As the direct beam passes through the sample, wavelengths that satisfy the Bragg conditions are scattered out of the beam. If the sample *is not* a perfect single crystal, then the overall image from the pencil-beam/sample-intercept volume can be thought of as being composed of distinct Laue images from subgrain volumes along the beam path (Fig. 2).

The overlapping Laue images from the subgrain volumes intercepted by the beam are resolved by the introduction of a differential aperture.[15] As illustrated in Fig. 2 b, when a highly absorbing wire is passed near the sample surface, it intercepts x-rays coming from the scattering volumes; if the wire is moved in small steps, the difference between the pattern before and after a move arises from those rays that pass near the edges of the wire. By projecting back from individual pixels past the wire edges, the intensity distribution into each pixel can be reconstructed from along the length of the beam path. This method can have submicron resolution even with large pixels due to the large ratio of the wire-to-detector compared to the wire-to-sample distances. Automated programs now exist to determine the Laue patterns as a function of sub-surface depth into the sample, and methods to accelerate differential aperture microscopy based on multiple wires or coded apertures are under development.[16]

Once the Laue patterns are determined along the beam path, it is possible to index the patterns and if the *undeformed* unit cell shape is known, determine the deviatoric ***elastic*** strain tensor.[17] This indicates the non-hydrostatic strain. The full strain tensor can be determined if the energy of one reflection is measured.[17] Polychromatic microdiffraction beamlines typically have special monochromators that allow them to switch between white-beam and polychromatic-beam conditions to make this measurement.[18-20]

As described above, each position in a Laue pattern is actually a weighted radial line integral through reciprocal space (Fig. 1). The line integrals are weighted by the intensity distribution over the bandpass of the x-ray probe and are sensitive to the integrated intensity along radial lines through reciprocal space. For materials with uniform elastic strain and negligible densities of unpaired (geometrically necessary) dislocations, Laue patterns have sharp spots. The overall Laue pattern can be used to determine the local phase[20], and the pattern can also be used to determine the local orientation. Typically orientations for samples with sharp spots can be determined to 0.01º and in some cases orientations to 0.001º are possible.

In most materials however, there is a combination of elastic and plastic deformation that complicates the measurement of both the elastic strain and the dislocation tensors. When either an elastic strain gradient or unpaired (geometrically necessary) dislocations are present, the sharp Laue spots are streaked. If the spatial resolution is sufficient to provide single-crystal-like local Laue images, then the elastic strain can be calculated from the local Laue image, and the local dislocation tensor can be calculated from neighbor crystallographic orientations (Eq. 2).

Although the local elastic strain/stress and the dislocation tensors can often be determined unambiguously (with sufficient technical care) it is also possible to extend the analysis of local defects through modeling. For example, various possible unpaired dislocation combinations can be fit to the experimental data to provide insights on the possible *dislocation systems* contributing to the local crystal deformation.[21-23] Beyond this level of materials characterization, it is in principle possible to characterize the unpaired dislocation density based on subtle changes to the diffuse scattering near the Laue reflections.[23] In practice this has not yet been demonstrated. The information that can be recovered by polychromatic microdiffraction is summarized in Fig. 3.

Scanning techniques

Several variants of polychromatic microdiffraction are made possible by standard polychromatic instrumentation. In addition to differential aperture scanning methods, monochromatic energy (wavelength) scanning methods can sometimes extend the capabilities of polychromatic microdiffraction to particularly challenging samples. For example, by scanning energy it is possible to determine reciprocal space points in 3 dimensions for unknown phase identification[24] and with calibration for integrated reflectivity information on each Laue spot. Similarly in highly strained materials monochromatic scans through reciprocal space allow for accurate determination of the local lattice parameters when streaking in white-beam measurements is too extreme to allow for accurate strain tensor measurements.

Facilities

The basic components for polychromatic microdiffraction are illustrated in Fig. 4. There are five key elements: (1) a brilliant synchrotron source; (2) an insertable nondispersive microbeam monochromator; (3) nondispersive focusing optics; (4) a precision sample stage; and (5) an x-ray sensitive area detector. Polychromatic microdiffraction facilities that resolve in three dimensions also have a differential aperture (6).

Several facilities dedicated to polychromatic microdiffraction are currently in operation with more coming on line over the next few years. At the Advanced Light Source, station 7.3.3 was probably the first dedicated polychromatic microdiffraction beamline.[19] This beamline used the broad bandpass from the ALS bend magnet source as a white beam. An intermediate focus at an adjustable slit provided a convenient method of adjusting the beam size and the beam could be rapidly cycled between a polychromatic and a monochromatic beam using a specially-designed nondispersive 4-crystal monochromator (Fig. 5b). Owing to the rapid drop in x-ray source intensity above 12 keV, this station was best suited for near surface, 2D studies of crystalline structures. Recently the microdiffraction station has been moved to a wavelength shifter, which increases the number of Laue spots and makes the beamline more suitable for differential aperture microscopy by providing a higher-energy spectrum.

Station 34-ID-E at the Advanced Photon Source is the first beamline with dedicated differential aperture microscopy capabilities.[25] This beamline was developed following a

successful demonstration on the APS beamline 7-ID. The type A source can be viewed either on axis for maximum monochromatic flux or off axis to smooth the spectra. The relative brilliance of beamline 34 is compared in Fig. 6 to other sources and illustrates the advantage of operation on a high-energy undulator. The optics of station 34-ID-E are very simple and include just the basic elements shown in Fig. 4. The undulator is typically adjusted to set the broad second harmonic at ~15 keV which provides a good combination of a large number of reflections and reasonable reflectivity. As illustrated in Fig. 6, the average off-axis brilliance for 34-ID is approximately two orders of magnitude greater than the average brilliance of a superbend source on the ALS or a bend magnet source on the on the Australian Light Source.

Station 34-ID-E utilizes a special two-crystal monochromator (5a) with the second crystal heated to align the monochromatic and polychromatic image positions.[18] This geometry is acceptable for the > 40 m long source distance of this beamline but is not appropriate for beamlines where the monochromotor is closer to the source.

The VESPERS beamline at the Canadian Light Source (CLS)[20] is a new polychromatic microdiffraction and fluorescence beamline built to allow for simultaneous diffraction and fluorescence microscopy. This beamline uses a pair of vertical focusing/deflecting mirrors together with a two-crystal monochromator to align the polychromatic and monochromatic beams (Fig. 5c). This new approach allows the robust simplicity of a two-crystal monochromator to be used on a beamline with a relatively short distance between the monochromator and the source.

In addition to these beamlines, there are polychromatic microdiffraction capabilities at the Swiss Light Source (SLS), the National Synchrotron Light Source (NSLS) with additional facilities under development at SOLEIL, the ESRF, and the Australian Light Source.

Example Applications

Inhomogeneous subgrain rotations during deformation

Measurements of near-grain-boundary and inhomogeneous intra-grain deformation in polycrystalline Ni tensile samples provide good examples of how polychromatic microdiffraction can provide new and quantitative information about materials behavior. In these studies, the misorientation near and across grain boundaries is measured before and after deformation. These experiment test the role of grain boundaries and free surfaces on inhomogeneous deformation, the role of grain boundaries on dislocation motions and how these behavior go beyond traditional explanations of texture development.

It is well known-for example- that grains rotate during deformation and that the pattern of rotations leads to the development of preferred crystallographic orientation (texture). This behavior can be reproduced using simple models based on the initial grain alignment and the deformation axis; grain alignment and applied stress direction determine the activated

slip systems. Grain-average (statistical) tests of existing models have been extensively conducted using x-ray and neutron techniques. These studies compare how stresses are accommodated (on average) in grains of a particular orientation or how different phases share an applied load.[26-28] They can also test how stress is distributed in fine-grained as compared to coarse-grained samples. Although these measurements are extremely useful for understanding trends in the materials response to deformation, they cannot capture the effect of *local* misalignments and structure. More recent high-energy monochromatic diffraction experiments have tested the behaviors of individual grains.[7-9] Measurements of the local environmental effects have however simply not been possible until now.

To begin to address this lack of direct experimental data, Pang et al.[29] have recently studied how neighbor grains respond across and near grain boundaries. As might be expected, if the grains are well aligned, they should rotate about the same amount, whereas grains that are highly misaligned should rotate different amounts and possibly in different directions. Fig. 7 illustrates the experimental setup. Samples with an average grain size of 30 μm were prepared from 99.97% pure Ni. Tensile specimens with dimensions of 8 mm in length by 300 μm thick were fabricated by electron discharge cutting. The sample surface was mechanically and then electrochemically polished.

The sample was probed by a polychromatic x-ray beam with an energy range of ~ 8-25 keV. The "diffracted volume" was a parallelepiped defined by the beam cross section and the penetration depth. Depth resolution was achieved using the differential aperture microscopy method developed by Larson et al.[10] The volumetric resolution of the measurements is 0.5(W) x 0.5 (H) x 1.0 (D) μm^3 and Laue images were collected down to ~30 μm beneath the surface. Indexing of these images yields the local grain orientation tensor. The grain boundaries along the diffracted volume were signaled by an abrupt change in the local orientation.

Measurements concentrated on regions near triple junctions and grain boundaries and near the centers of individual grains. Local orientations along the lines through the pre-selected positions were probed at 0% and 8% plastic strain. Orientations were determined with a precision of <0.02º at 0% strain. As dislocation density increases with deformation the angular resolution dropped to ~0.1º at 8% strain due to degradation of the peak shapes.

The grain-boundary-surface normal and grain boundary angle, θ, between adjacent grains were determined by the orientation tensors measured at the center of each grain.[30] Among the 49 grains measured there are 120 grain boundaries, and 17 of them are low angle (<15º) boundaries. The remaining boundaries are high-angle boundaries with 16 special boundaries having CSL=1,3,9 or 27. Low-angle and special grain boundaries have the tendency to cluster together forming 'special' triple junctions. Nine out of the 66 triple junctions are special triple junctions.

For the grain boundary and triple junction regions, *misorientations* of volume elements across grain boundaries were calculated. Fig. 8 plots the *change* in misorientation, ω, *after* deformation as a function of original misorientation, θ, *before* deformation. From

Fig. 8 it is clear that typically larger *original* misorientation, θ, leads to larger *changes* in misorientation, ω, after deformation. This behavior is easy to understand in light of the tendency of grains with different crystallographic orientation to rotate in different directions. The small ω observed in low-angle and near special grain boundaries and triple junctions suggests that these intercrystalline regions introduce only minor obstacles to dislocation motion. This is direct evidence to explain why specimens with a high density of special boundaries and special triple junctions have lower tensile strength and are more ductile. The large ω found in high-angle intercrystalline regions suggest that they are more effective in raising flow stresses as observed in macroscopic measurements.[31] This behavior is consistent with a "rind" or "core" model for intra-granular deformation which predicts largest increases in lattice curvature near the grain boundaries.[32]

To further study how misorientations are accommodated inside single grains, measurements were made on a sample with larger grain size; the 99.96% pure Ni sample had an average grain size of ~200 μm and the dimensions of the sample are shown in Fig. 9. The sample was vacuum annealed at 800º C for 4 hours. Polychromatic microdiffraction measurements were made on station 34-ID-E at the APS. Measurements were made on four grains labeled A-D and highlighted in Fig. 9. The measurements were made with a beam with a cross-section of 0.46 x 0.55 μm^2. The beam penetrated ~ 30 μm beneath the surface normal. An orientation map collected at 0% strain over a region of 4 × 0.5 mm^2 with a step size of 5 μm around the center of the sample is overlaid on the overall sample profile (Fig. 9).

Laue patterns were collected at the center of each grain at 0%, 10% and 15% strains. The Laue peaks are highly streaked at 10% and 15% deformation. Indexing of the streaked patterns is difficult, as the changes of orientation due to unpaired dislocation accumulation within the integrated depth of the gauge volume (~ 30μm) are much larger than the angular resolution of the CCD. Depth-resolved profiling was carried out at these four positions to determine the local Laue diffraction contributed at specific depths beneath the surface.

Laue patterns for all grains indicate the presence of streaks, however the streaked pattern of each grain is different as it is dependent on the distinct dislocation activities within the grains. Depth-resolved information was obtained by reconstructing depth-specific images collected with the differential-aperture method. The peaks in the reconstructed images from the deformed sample are not as perfect as those found at 0 % strain. This suggests the deformation microstructure is finer than the 1 μm depth resolution. The orientation tensor of each sampling volumes was determined from the reconstructed images.

The shape of the observed Laue streaks is interpreted by simulations of the diffracted Laue patterns and determines the scalar dislocation density distribution η. Deformation of the grains was described by the formation of GNDs and GNBs. For Ni, an FCC material, edge dislocation lines (ξ) are typically parallel to <112> with <110> Burgers vector (**b**) and [111] glide planes. Depth-resolved images were simulated with a series of slip systems combinations. The slip systems were then determined by comparing the

simulations with the experimental results. Figure 10 depicts the best-fit simulation pattern for grain A at 5μm in depth with **b** // $[01\bar{1}]$ and ξ // $[2\bar{1}1]$. Splitting of "streaked" patterns was observed as depth increased. This indicates that at least two different slip systems combinations are present through the depth of the grains. For grain A, simulations show that combination of two slip systems of **b** // $[01\bar{1}]$ and ξ // $[21\bar{1}]$and **b** // $[0\bar{1}1]$ and ξ // $[\bar{2}1\bar{1}]$ give a better fit to the experimental data.

Electromigration

Electromigration is another good example of how inhomogeneous grain and subgrain deformation is ubiquitous in materials behavior and how polychromatic microdiffraction can provide new information. Indeed, one of the most compelling motivations for the development of polychromatic microdiffraction was a need to measure *elastic* strain in interconnects in situ, under a SiO_2 passivation layer. Some of the first polychromatic microdiffraction experiments were performed on interconnect samples wherein addition to elastic strains, lattice curvatures were detected and attributed to unpaired dislocations.

Electromigration is the process of mass transport due to electrical current flow. Although the phenomena has been long recognized, electromigration has attracted increased attention due to the continuing decrease of the current carrying "interconnect" line dimensions in integrated circuits. Decreasing interconnect cross sections have driven current densities toward ~1 MA/cm^2 where electromigration is a serious limitation for device reliability.

Although much is understood about electromigration, polychromatic microdiffraction is providing important new insights. Electromigration is known to arise from the momentum imparted by moving electrons, by the local electric field and by heat-accelerated mobility of mass and surface diffusion. A schematic of electromigration in a CuAl interconnect is shown in Fig. 11. Interconnect behavior during electromigration has- until recently- been modeled primarily assuming the development of the elastic strain fields that inhibit additional mass transport.[33-37]

Recent experiments with polychromatic microdiffraction have now shown that in addition to elastic strains, plastic deformation arises during electromigration and may play an important role in the eventual failure of interconnects.[35-39] Experiments were performed primarily on beamline 7.3.3 at the Advanced Light Source. The interconnect samples consisted of patterned Al (0.5% wt. Cu) lines sputtered deposited on Si and buried under a glass passivation layer (0.7 μm thick). The lines had a length of: 30 μm, a width 4.1 μm, and a thickness 0.75 μm. Electrical connections to the line were made through unpassivated Al (Cu) pads connected to the sample through W vias. Details on the experimental setting and data collection can be found elsewhere.[36-40] Measurements of interconnect lines before electromigration typically found sharp diffraction spots indicating that the grains of the interconnect had few unpaired dislocations (Fig. 12a).

During electromigration, the Laue patterns change depending on grain size, and position along the interconnect line. A typical response is shown in Fig. 12b. Several trends were noted:

(1). Deformation was larger in big grains.
(2). Small grains rotate.
(3). Deformation is preceded by Cu diffusion which evaporates “hardening” precipitates near the cathode end of the interconnect and grows precipitates near the anode end of the interconnect.
(4). Near the middle of the interconnect, unpaired dislocations initially develop parallel to the electrical field.
(5) Little dislocation activity is observed near the anode end of the wire (Cu enhanced).

Models of electromigration must now take into account these observed behaviors in schemes to improve interconnect reliability. Barabash et al. have proposed mechanisms to explain the observed grain behavior.[38-40]

Plastic deformation near welds

Welding is another critical materials technology where inhomogeneous deformation plays a crucial role. In welded parts, the strength of the final product is often determined by the welded material and not by the base metal. During welding, the local micro and meso structure of materials can be greatly modified, and depending on the process, the grain size can be increased or decreased, new phases can be introduced, and/or the material can be left with significant residual stress and plastic deformation. Polychromatic microdiffraction measurements have already been made on fusion welds[41-43], spot welds, and friction-stir welds[44]. Here we briefly describe observations made on Ni-based super alloy fusion welds. A typical fusion weld[45] is illustrated schematically in Fig. 13.

In a fusion weld, two parts are brought into close proximity, and the joint between two parts is raised to a sufficiently high temperature to melt the interface. There are three important zones: (1) the original base material that is far enough from the weld that it not affected by the welding process; (2) the heat affected zone where plastic deformation and residual stresses are introduced into the grains; and (3) the fusion zone where the base material hardens after being heated into a liquid and subsequently solidified. In addition weld scientists refer to the fusion line along the boundary between the heat-affected zone and the fusion zone and the centerline that defines the geometrical center of the weld.

In-situ real time measurements of welds have found that during solidification, welds may exhibit transient phases [46-48], and it is well known that dendritic growth during solidification leads to inhomogeneous chemistry and possible multiple phases in alloy welds. X-ray and neutrons studies have also identified the development of residual stress in welded materials.

Polychromatic microdiffraction has the ability to probe grains within the various zones and finds strikingly different deformation behavior in the different zones. We have analyzed the local dendrite-to-dendrite microstructure of the FZ and HAZ in RENE-5 nickel-based single-crystal superalloy welds. The surface normal was in the [310] direction. Chemical composition of the alloy is shown in the table
Table

Alloy	Cr	**Ti**	Mo	W	Re	**Ta**	**Al**	Co	Hf	B	C	Σ
Rene N5	7.0	**1.0**	2.0	5.0	3.0	**7.0**	**6.2**	8.0	.15	.004	.05	17.0

As illustrated in Fig. 14, for this Ni-base super alloy weld, the Laue spots are sharp near the weld centerline, but grow near the fusion line. Largest deformations are in fact observed in the HAZ and close to the FL of the weld. The observed behavior is believed to result from the formation of inhomogeneous stresses, lattice rotations, and plastic deformation in different zones of the weld.[41-43] Dissolution of the γ' - phase particles during heating and secondary precipitation of γ' during cooling is found, as well as formation and multiplication of dislocations. In the immediate vicinity of the FL, the spatial and temporal temperature gradients are maximized, which causes the formation of a high density of dislocations. Dislocations are concentrated in the γ matrix of the single crystal superalloy.

Plastic deformation in single crystals

Although it is clear that the presence of grain-boundaries, free surfaces and other interfaces play critical roles in the deformation of polycrystalline materials, the behavior of even single crystals is currently beyond the scope of existing theory. Larson et al.[49] have recently reported 3D measurements of deformation formation in perfect Cu single crystals by nanoindentation. These measurements can be directly compared to theoretical models, as the small volume of deformation can be both experimentally interrogated with polychromatic microdiffraction and can be theoretically modeled. Furthermore the measurements are highly reproducible and include well-understood boundary conditions. Other 3D measurements of single crystal Cu during tensile measurements[50] are also underway. These measurements tie direct to the extensive body of surface measurements.

Future

The main drawback to differential aperture microscopy is the time required to map three-dimensional volumes. Area detectors employed at current facilities require about 2-8 seconds to readout an image. At best it takes at least one image for every volume element (voxel) of reconstructed data. In practice about 50-100 reconstructed depth-profiled images can be determined in 15 minutes (~10 seconds/voxel). More than 115 days are therefore required to map a volume resolved into 100x 100 x 100 voxels and even a single internal surface with 100 x 100 voxels requires about 1 day of measurements. However, on station 34-ID-E the data collection time required can be ~10 msec and could be made even shorter with slightly more efficient optics. The actual data collection time required for 10^6 voxels, is therefore less than 3 hours, ~10^3 faster than experimentally

realized. To reach this goal, much faster detectors will soon be deployed on beamline 34. With 10-100 frames/second readout, we anticipate the ability to produce photograph quality images of tensor element distributions in 3D. This will enable a new capability: the ability to search for interesting physical features inside a sample, and then to follow the mesoscale structural evolution through processing steps. This will also allow for careful tests of mesoscale deformation models that include boundary conditions before during and after mesoscale evolution. When rapid readout capabilities are coupled with energy-sensitive x-ray pixilated arrays, it will be possible to accurately determine the local stress tensor rapidly without the need for monochromatic scanning. This additional feature will further evolve polychromatic microdiffraction into an indispensable tool for understanding inhomogeneous deformation. In addition, the technology exists to produce far smaller beams than are presently employed. Beams around 20 nm will allow for nondestructive measurements of embedded nanoscale structure on a length scale that will provide a direct link to atomic scale models.

Acknowledgement

This research supported by the Division of Materials Science and Engineering, U.S. Department of Energy. Experimental measurements performed in part on beamline 34-ID at the Advanced Photon Source, and on beamline 7.3.3 at the Advanced Light Source. The U.S. DOE Office of Basic Energy Sciences, Office of Science, supports both beamlines.

"The submitted manuscript has been authored by a contractor of the U.S. Government under contract No. DE-AC05-00OR22725. Accordingly, the U.S. Government retains a nonexclusive, royalty-free license to publish or reproduce the published or reproduce the published form of this contribution, or allow others to do so, for U.S. Government purposes."

References

1. Y. Xiang, "Modeling dislocations at Different Scales", *Commn. in Comput. Phys.* **1** 383-424 (2006).

2. N. Hansen, " Boundary Strengthening over five Length Scales", *Adv. Eng. Mat.* **7** 815-821 (2005).

3. J. F. Nye, *Acta. Metall.* **1** 153 (1953).

4. I.C. Noyan and J.B. Cohen, **Residual Stress**, pg. 34 Springer-Verlag, New York (1987).

5. J. Weertman and J.R. Weertman, **Elementary Dislocation Theory**, Macmillan Company, New York, (1964).

6. L. Margulies, G. Winther, H.F. Poulsen, "In situ measurement of grain rotation during deformation of polycrystals", *Science* **291** 2392-2394 (2001).

7. H.F. Poulsen, L. Margulies, S. Schmidt and G. Winther, "Lattice rotations of individual bulk grains-art I: 3D X-ray characterization", *Acta Materialia* **51** 3821-3830 (2003).

8. G. Winther, L. Margulies, S. Schmidt, and H.F. Poulsen, " Lattice rotations of individual bulk grains Part II: correlation with initial orientation and model comparison", *Acta Materialia* **52** 2863-2872 (2004).

9. G. Winther, L. Margulies, H.F. Poulsen, S. Schmidt, A.W. Larsen, E.M. Lauridsen, S.F. Niesen, and A. Terry, " Lattice rotations of individual bulk grains during deformation", *Mat. Sci. Forum* **408** 287-292 (2002).

10. B.C. Larson, A. El-Azab, W. Yang, J. Z. Tischler, W. Liu, and G. E. Ice, "Experimental Characterization of The Mesoscale Dislocation Density Tensor," *Philosophical Magazine*, **87**, 1327-1347 (2007).

11. S.F. Nielsen, E.M. Lauridsen, D.J. Jensen and H.F. Poulsen, " A three-dimensional X-ray diffraction microscope for deformation studies of polycrystals", *Mat. Sci. and Eng*. **319** 179-181 (2001).

12. M. von Laue, "Concerning the detection of X-ray interferences", *Nobel Lecture* (1915).

13. B.E. Warren, X-ray Diffraction, Dover Pub., New York, pg. 19 (1990).

14. G.E. Ice, J.-S. Chung,J.Z. Tiscler, A. Lunt, and L. Assoufid,,"Elliptical x-ray microprobe mirrors by differential depostion", *Rev. Sci. Inst.* **71** 2635-2639 (2000).

15. B. C. Larson, W. Yang, G. E. Ice, J. D. Budai, and J. Z. Tischler, "Three-Dimensional X-Ray Structural Microscopy with Submicrometre Resolution," *Nature* **415**, 887 (2002).

16. J.S. Chung, S. Isa, V. Greene, O. Broadwater, W. Liu, and G.E..Ice, "Multiple differential-Aperture Microscopy, *Nuc. Inst. & Meth A*, accepted (2007).

17. J. S. Chung and G. E. Ice, "Automated Indexing for Texture and Strain Measurements with Broad-Bandpass X-ray Microbeams," *J. Appl. Phys*. **86**, 5249-5256 (1999).

18. G. E. Ice, J.-S. Chung, W. Lowe, E. Williams, and J. Edelman, "Small-displacement Monochromator for Microdiffraction Experiments," *Rev. Sci. Inst.* **71**, 2001-2006 (2000).

19. A.A. MacDowell, R.S. Celestre, N. Tamura, R. Spolenak, B. Balek, W.L. Brown, J.C. Bravman, H.A. Padmore, B.W. Batterman, J.R. Patel, " Submicron X-ray diffraction", *Nuc. Inst. and Meth. A*, **467** 936-943 (2001).

20. R. Feng, A. Gerson, G. Ice, R. Reininger, B. Yates, and S. McIntyre, "VESPERS: A Beamline for Combined XRF and XRD Measurements, *AIP Conf. Proc*. **879** 872-874 (2006).

21. R. I. Barabash, G.E. Ice, and F.J. Walker, "Quantitative microdiffraction from deformed crystals with unpaired dislocations and dislocation walls", *J. Appl. Phys*. **93** 1457-1464 (2003).

22. Barabash, R., Ice, G.E., Pang, J. W. L., and Liu, W., "Characterization of the Dislocation Density Tensor with White Beam Diffraction," *TMS Letters* Vol. 1 13-14, 2004.

23. R. I. Barabash, G. E. Ice, and J. W. L. Pang, "Geometrically Necessary Dislocations from White Beam Microdiffraction," *Mater. Sci. Eng A* **400**, 125 (2005).

24. E. Miura, G. E. Ice, E. D. Specht, J.W.L. Pang, H. Kato, K. Hisatsune, and I. Inoue, "X-ray Study of $Pd_{40}Cu_{30}Ni_{10}P_{20}$ Bulk Metallic Glass Brazing Filler for Ti-6Al-7Nb Alloy," *Materials Science Forum*, **539-543** 1983-1987 (2007.

25. G. E. Ice and B. C. Larson, "3D X-ray Crystal Microscope," *Adv. Eng. Mat*. **2**, 643-646 (2000).

26. J.W. L. Pang, T.M. Holden, and T.E. Mason, "In-situ generation of intergranular strains in an A17050 alloy", *Acta Materialia*, **46** 1503-1518 (1998).

27. J.W.L. Pang, T.M. Holden, and T.E. Mason, "The Generation of Intergranular Strains in 309H Stainless Steel under Uniaxial Loading", *Acta Mater*. **48** 1131 (2000).

28. P.J. Withers and A.P. Clarke, "A neutron diffraction study of load partitioning in continuous Ti/SiC composites", *Acta Mater*. **46** 6585 (1998).

29. J.W.L. Pang, R. Barabash, W. Liu and G.E. Ice, " Determination of Deformation Inhomogeneity in Polycrystalline Ni under Uniaxial Tension with 3D X-ray Microscope", *TMS Letters*, **1** 5 (2004).

30. W.J. Liu, G.E. Ice, B.C. Larson, W. Yang and J.Z. Tischler, "Nondestructive three-dimensional characterization of grain boundaries by X-ray Crystal Microscopy", *Ultramicroscopy* **103** 199 (2005).

31. Y. Zhou, U. Eb, K.T. Aust, G. Palumbo, "The effects of triple junctions and grain boundaries on hardness and Young's modulus in nanostructured Ni-P", *Scripta Materialia* **48** 825 (2003).

32. J.A. Wert, X. Huang, G. Winther, W. Pantleon and H.F. Poulsen, "Revealing deformation microstructures", Mat. Today, 10 24-32 (2007).

33. R. Spolenak, O. Kraft, and E. Arzt, "Alloying effects in electromigration: What controls the electromigration draft?",*AIP. Con. Proc*. **491** (1999) 126-137.

34. C. Witt, C. Volkert, E. Arzt, "Electromigration-induced Cu motion and precipitation in bamboo Al-Cu interconnects"*Acta Materialia* **51** (2003) 49-60.

35. P.-C. Wang, I. C. Noyan, S. K. Kaldor, J. L. Jordan-Sweet, E. G. Liniger, and C.-H. Ku, "Real-time x-ray microbeam characterization of electromigration effects in Al(Cu) wires", *Appl. Phys. Lett*., **78** (2001) 2712-2714.

36. C. Valek, N. Tamura, R. Spolenak, W.A. Caldwell, A.A. MacDowell, R.S. Celestre, H.A. Padmore, W.L. Brown, B.W. Batterman, W.D. Nix, and J.R. Patel, "Early stages of plastic deformation in thin films undergoing electromigration", *Appl. Phys. Lett*. **94** 3757-3761 (2003).

37. N. Tamura; R. Spolenak, B.C. Valek; A. Manceau; M. Meier Chang; R.S. Celestre; A.A. MacDowell; H.A. Padmore and J.R. Patel, "Submicron x-ray diffration and its applications to problems in materials and environmental science", Rev. of Sci. Instr. **73** 1369-1372 (2002).

38. R.I. Barabash, G.E. Ice, N. Tamura, B.C. Valek, J. C. Bravman, R. Spolenak and J.R. Patel, "Quantitative analysis of dislocation arrangement induced by electromigration in passivated Al (0.5wt% cu) interconnects", *J. Appl. Physics*, **93**, 5701-5706 (2003).

39. R.I. Barabash**,** G.E. Ice, N. Tamura, B.C. Valek, J. C. Bravman, R. Spolenak and J.R. Patel, "Quantitative characterization of electromigration-induced plastic deformation in Al(0.5% cu interconnect", *Microelectronic Engineering*, **75**, 24-30, (2004).

40. R.I. Barabash, G.E. Ice, N. Tamura, B.C. Valek, J. C. Bravman, and J.R. Patel, “White beam analysis of coupling between precipitation and plastic deformation during electromigration in a passivated Al (0.5 wt% Cu) interconnect”, *Metallofiz. Noveishie Teknol*. **27**, 75-94 (2005).

41. O. M. Barabash, J. A. Horton, J. S. Park, S. S. Babu, J. M. Vitek, S. A. David, G. E. Ice, and R. I. Barabash, "Evolution of dislocation structure in the heat affected zone of a nickel-based single crystal", *J. Appl. Phys.* ***96***, 3673 (2004).

42. O. M. Barabash, R. I. Barabash, S. A. David, G. E. Ice, "Residual Stresses, Thermomechanical Behavior and Interfaces in the Weld Joint of Ni-based Superalloys", *Advanced Engineering Materials*, **8**, 202-205 (2006).

43. O.M. Barabash, S.S. Babu, J.M. Vitek, S.A. David, G.E. Ice and R.I. Barabash**, "** Unusual Dislocation Density Oscillations after Local Melting and Solidification of Ni-based Superalloys", *TMS Letters*, **2**, 31-32 (2005).

44. O.M. Barabash, R.I. Barabash, G.E. Ice, S.A. David, Z. Feng, J. Horton, “X-ray MicroBeam Characterization of the Near Surface Nanostructured Layer in Ti after Friction Stir Processing”, *Reviews on Advanced Materials Science*, **14,** 14-34 (2007).

45. S. A. David, S. S. Babu, and J. M. Vitek, "Welding", In: *Encyclopedia of Materials: Science and Technology Updates*, Elsevier, Oxford, 1- 9 (2003).

46. J.W. Elmer, J. Wong, T. Ressier, " Spatially resolved X-ray diffraction mapping of phase transformations in the heat-affected zone of carbon-manganese steel arc welds", *Met. and Mat. Trans. A-Phys. Metall. and Mat. Sci*. **32** 1175-1187 (2001).

47. T.A. Palmer, J.W. Elmer and J. Wong, "In situ observations of ferrite-austenite transformations in duplex stainless steel weldments using synchrotron radiation", *Sci. and Tech. of Welding and Joining*, **7** 159-171 (2002).

48. S.S. Babu, J.W. Elmer, J.M. viteka and S.A. David, "Time-resolved X-ray diffraction investigation of primary weld solidification in Fe-C-Al-Mn steel welds", *Acta. Materialia* **50** 4763-4781 (2002).

49. M.E. Kassner, S.Nemat-Nasser, Z. Suo, G. Bao, J.C. Barbour, L. C. Brinson, H. Espinosa, H. Gao, S. Granick, P. Gumbsch, k.-S. Kim, W. Knauss, L. Kubin, J. Langer, B.C. Larson, L. Mahadevan, A. Majumdar, s. Torquato, F.van Swol, "New directions in mechanics", *Mech. of Mater*. **37** 231-259 (2005).

50. J.W.L. Pang, private communication

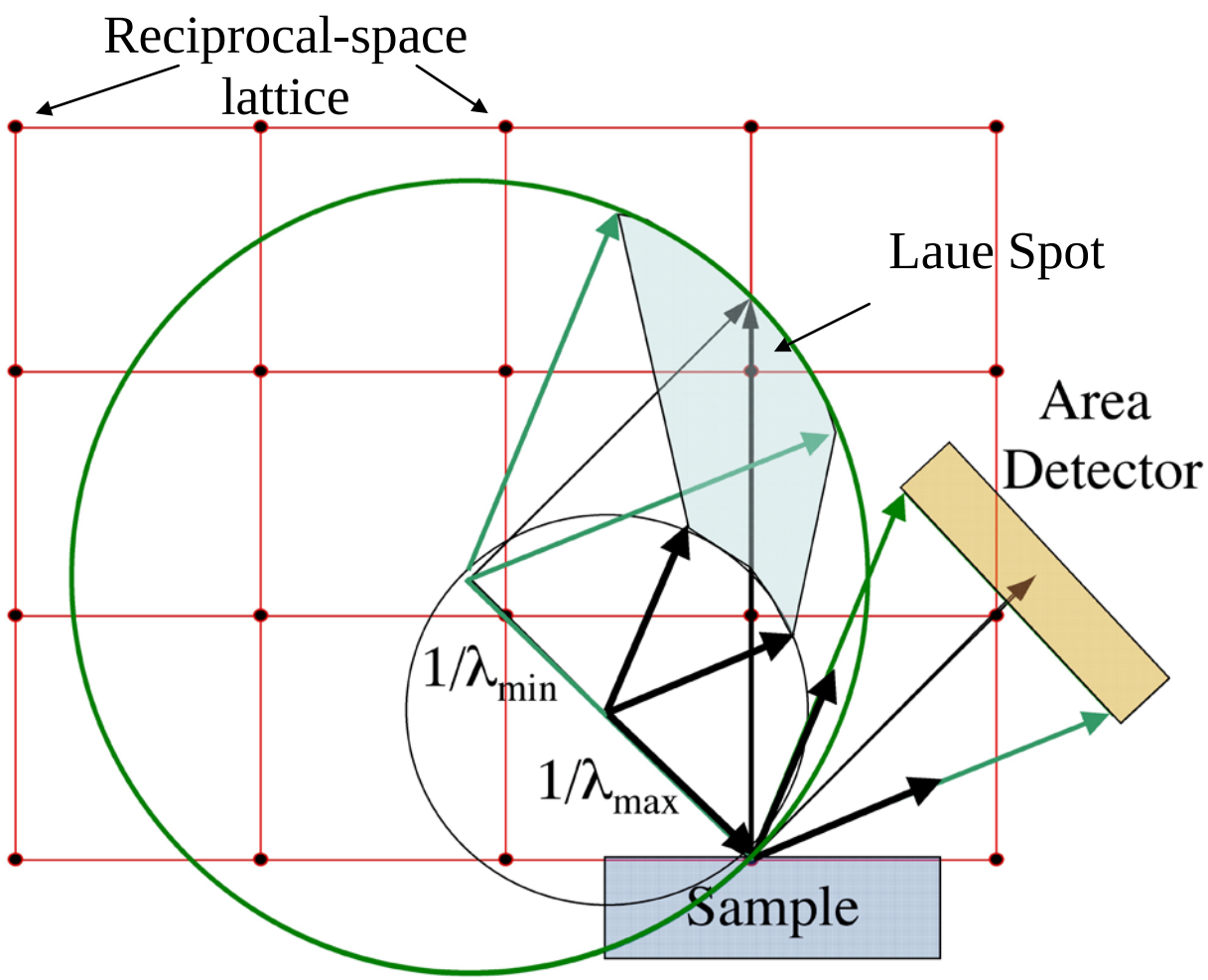

Fig. 1. A two-dimensional modified Ewald's sphere diagram. In reciprocal space, the momentum of an x-ray beam depends on its direction and wavelength. For short wavelength (green) the momentum is larger than for large wavelength (black). The momentum transfer is equal to the vector difference between the final and incident x-ray momentums. For a fixed wavelength all-possible momentum transfers lie on a sphere. The centers of the spheres for different wavelengths lie along the incident beam direction and touch at the 0,0,0 position (no momentum transferred). The Laue pattern observed by an area detector is made up of radial line integrals through reciprocal space. For a continuum source, lattice points that lie within the bounds of the minimum and maximum Ewald's spheres *and* which have scattered beams within the solid angle of the detector contribute to the line integral.

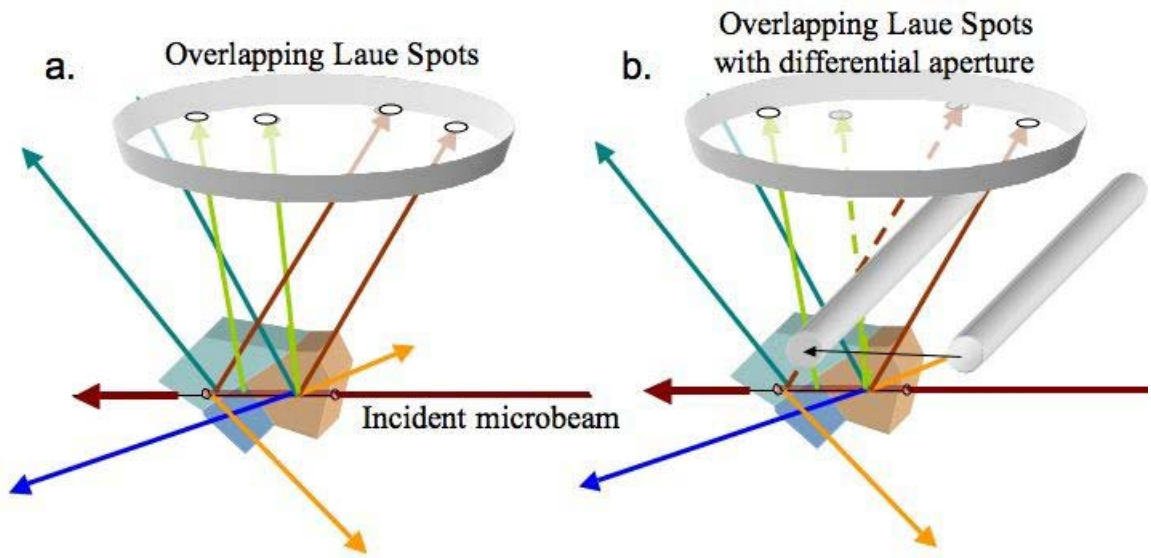

Fig. 2. As a polychromatic x-ray beam penetrates a crystalline sample, it generates Laue patterns from each subgrain along the beam. The Laue patterns overlap at the detector. The overlapping Laue patterns can be resolved by passing an absorbing wire near the sample surface; intensity from the sample that passes near the edge of the wire is either passed or occluded by small wire motions.

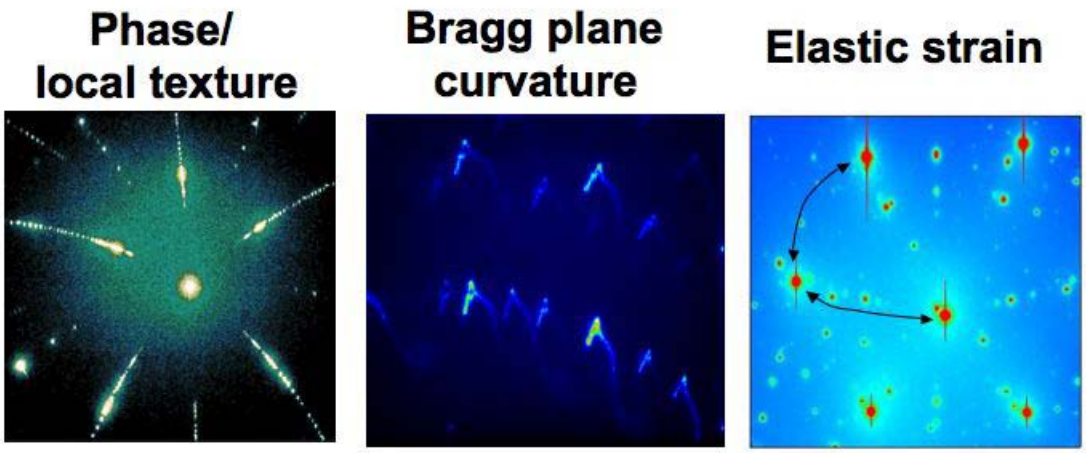

Fig. 3. (a). The number of reflections and symmetry can be used to identify phases. In addition, the orientation of the pattern can determine the local orientation of the grain(s). In the figure on the left, a GaN film is aligned to a SiC substrate. Small shifts in the relative orientation can be measured by zooming in on the Laue spots. (b). In this sample, the Bragg planes are curved and smear the Laue spots. (c). By measuring the angles between spots, it is possible to determine the local deviatoric strain tensor. If in addition, the energy of one spot is measured, then the full strain tensor can be determined.

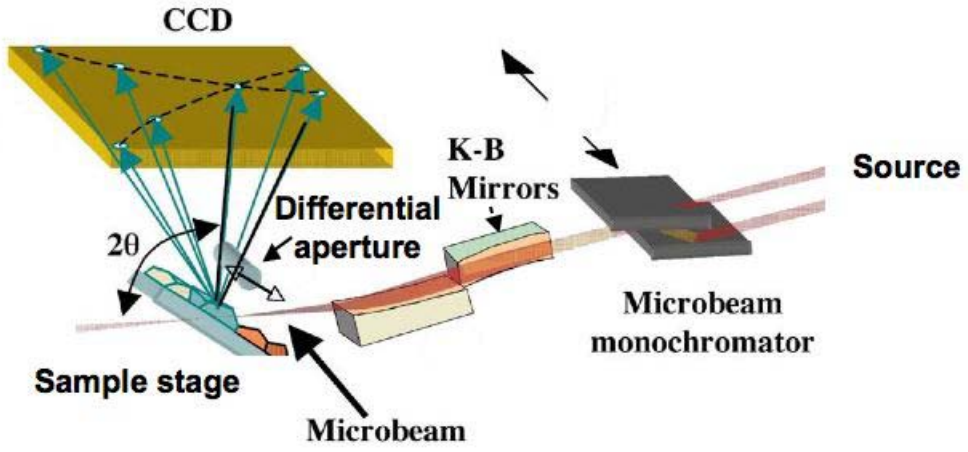

Fig. 4. The necessary parts of a polychromatic microdiffraction instrument are schematically illustrated. An intense source is used to pass either a polychromatic or a monochromatic beam onto the sample. The beam can be rapidly changed between a monochromatic beam and a polychromatic beam by inserting or removing a nondispersive monochromator. The beam is then focused with a nondispersive Kirkpatrick-Baez mirror system onto the sample. The sample is moved under the fixed beam with a precision sample stage. An x-ray sensitive CCD area detector collects the pattern. If the sample is resolved in 3 dimensions, then a wire that acts like a knife edge or differential aperture is passed near the sample surface.

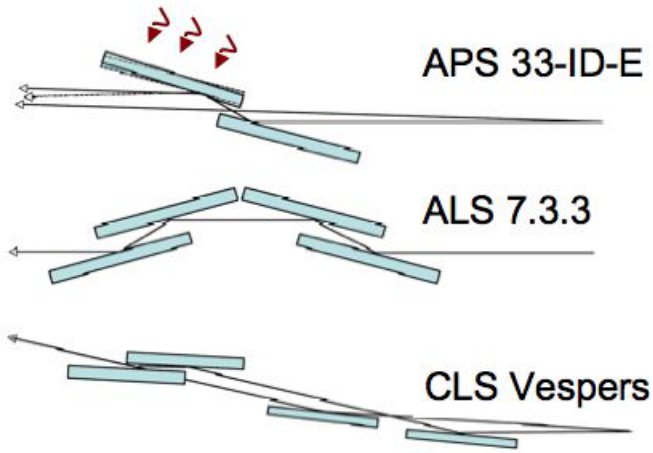

Fig. 5 Three schemes have already been employed to provide a nondispersive monochromator. At beamline 33-ID-E (top), the monochromator is ~40 m from the source and the beam displacement through the two-crystal system is about 1 mm (0.5 mm gap). The 25-microradian angular differences between rays that reflect off the monochromator compared to rays that pass the monochromator when it is removed is compensated by heating the second crystal, which optimizes the reflectivity at a slightly different Bragg angle. On beamline 7.3.3 (middle) a four-crystal system is used. The crystals are mounted so the beam can pass between the crystals when the crystal angle is set to near glancing conditions. On the VESPERS beamline two beams are deflected by upstream mirrors at slightly different angles. This compensates for the 100-microradian difference in the angles of the two beams before they reach the monochromator.

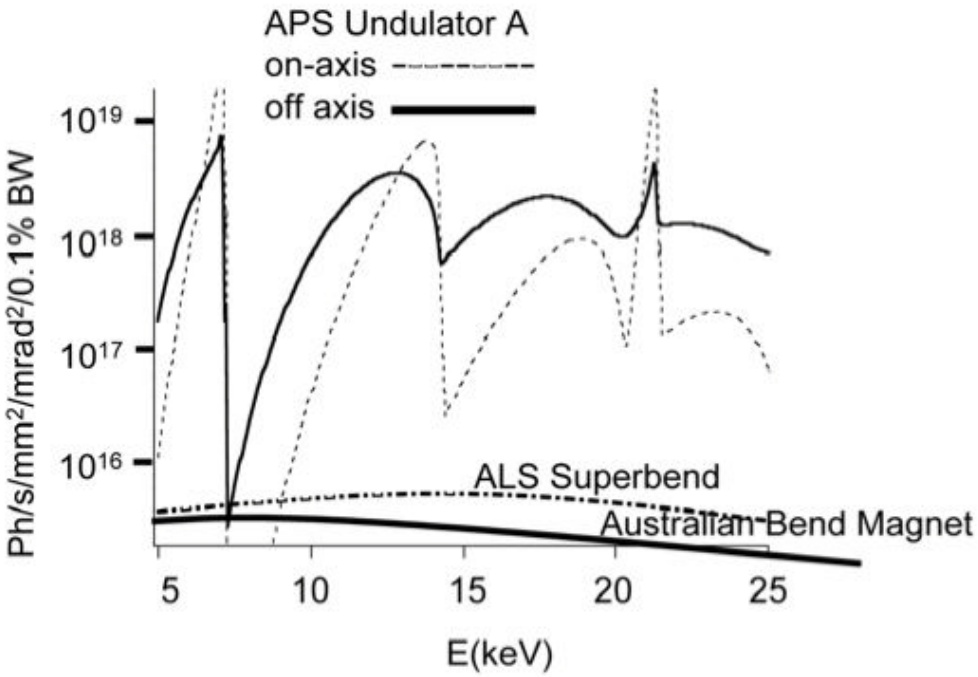

Fig. 6. The brilliance of an APS undulator A peaks at the harmonics. Highest monochromatic brilliance is achieved with the undulator on axis. However, even off axis, the brilliance between the harmonic peaks is two orders of magnitude higher than for a bend magnet or super bend magnet source. For polychromatic studies it is often useful to operate off axis where the spectrum is more uniform as a function of x-ray energy.

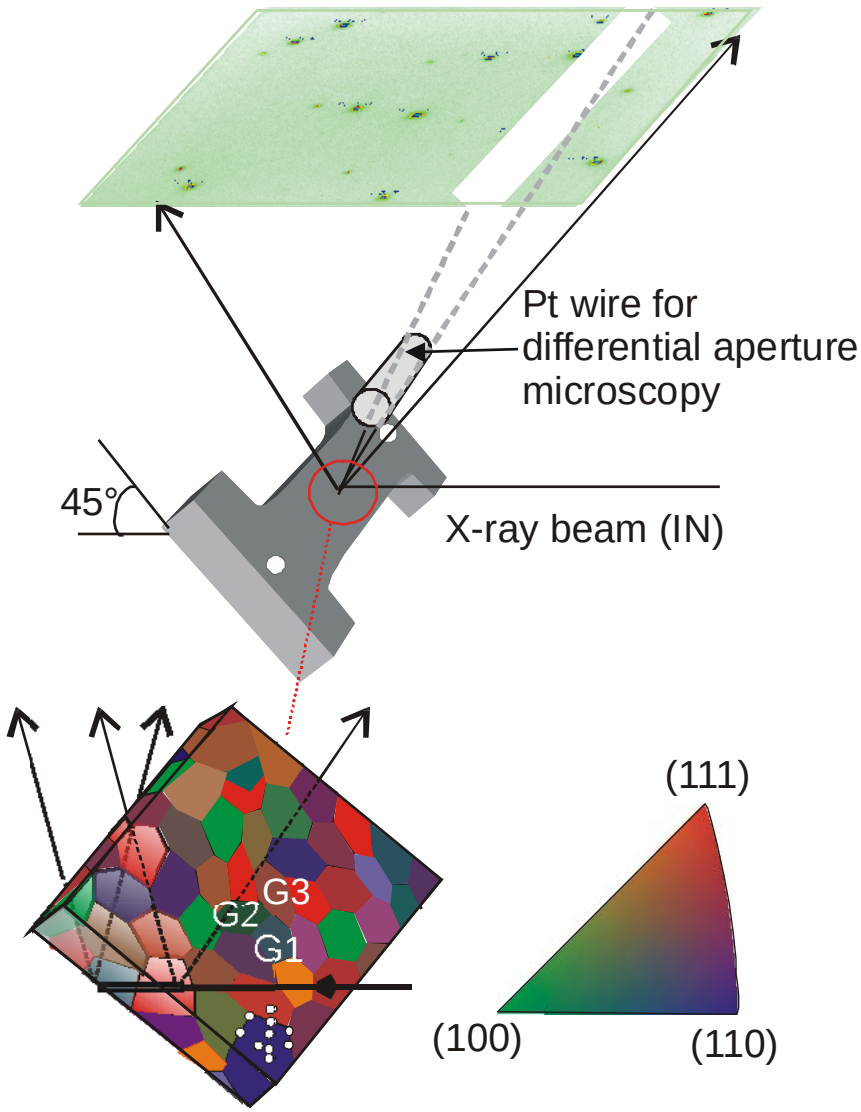

Figure 7. Schematic diagram of the experimental setup. The tensile sample is seated at 45° with respect to the incident polychromatic beam. Laue images are collected using a CCD. Orientations of the grains parallel to the tensile length are shown on the measured sampling regions with the color legend shown on the right. The regions of a grain selected for measurements are highlighted by white dots.

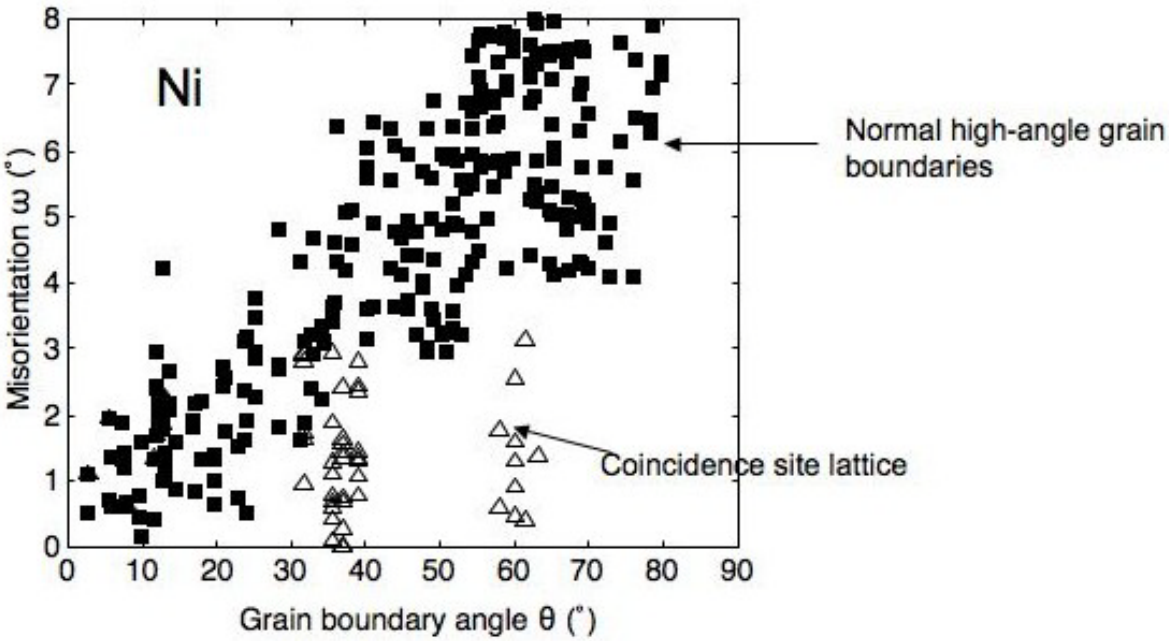

Figure 8. Plotted above is the distribution of *changes* in misorientation, ω, for all the measured volume elements lying in the intercrystalline regions as a function of the original grain boundary angle, θ. θ is defined as the misorientation between two neighboring grains before deformation. ω is defined as the misorientation between volume element in the grain boundary/triple junction region and the grain itself after 8% strain. The blue triangles are the measurements for the high angle low energy intercrystalline regions.

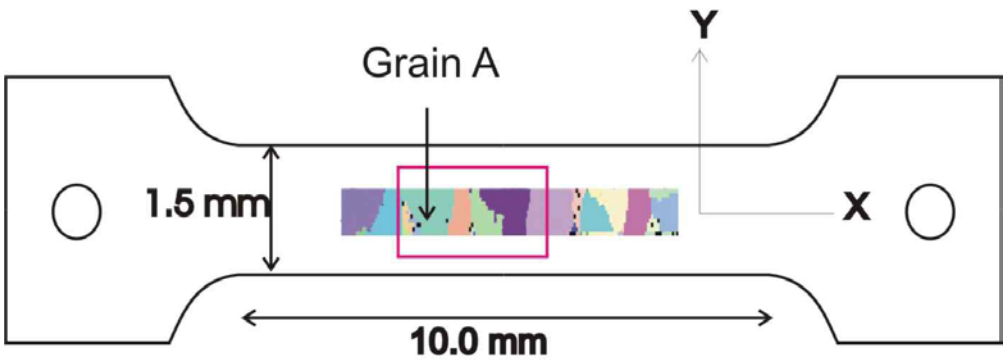

Figure 9. Dimensions of the tensile sample. The red box highlighted the four grains measured in the experiment.

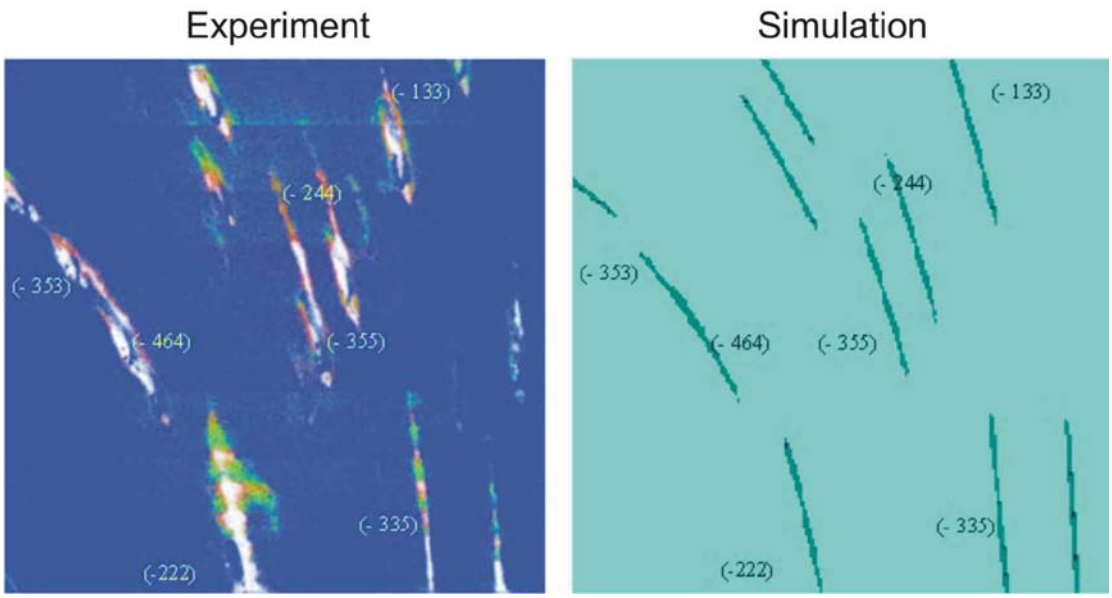

Figure 10. Comparison between experimentally obtained depth-resolved Laue images and the simulated images for depth = 15 μm.

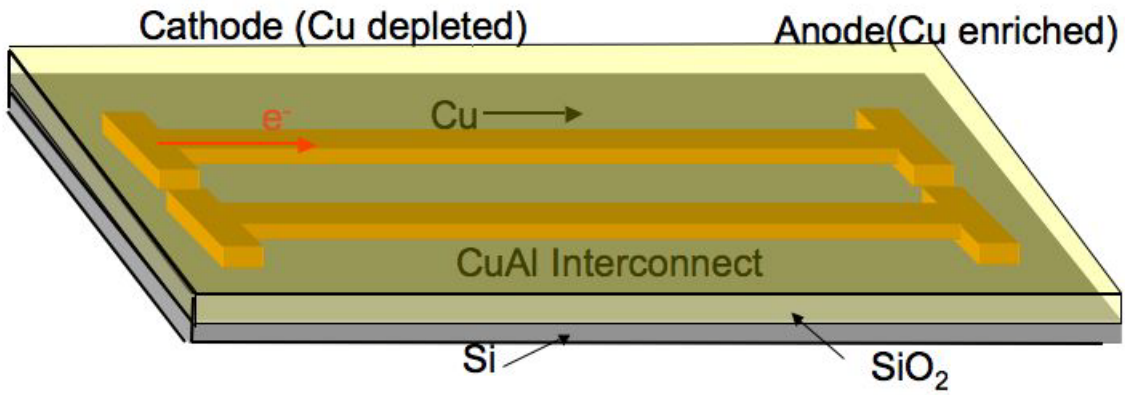

Fig. 11. Schematic of an electromigration test sample.

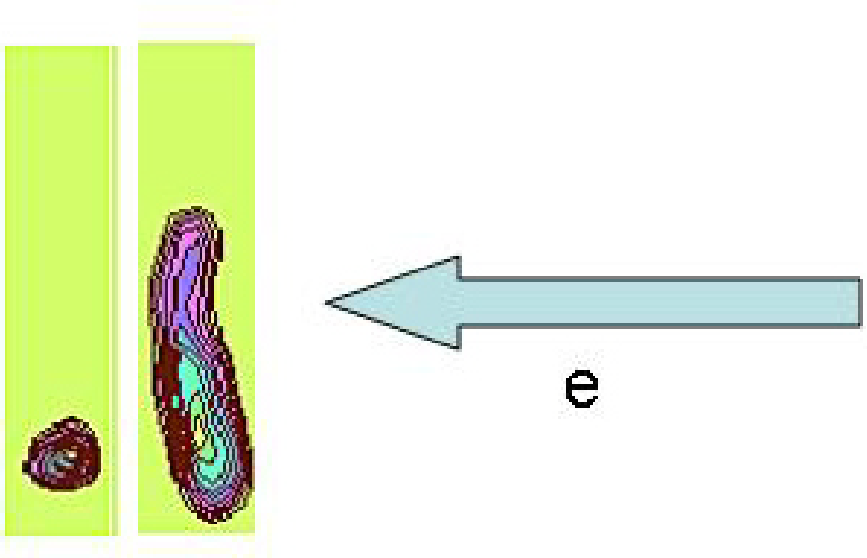

Fig. 12. (a) Laue spot before electromigration; (b) Laue spot after electromigration. Arrow shows current direction.

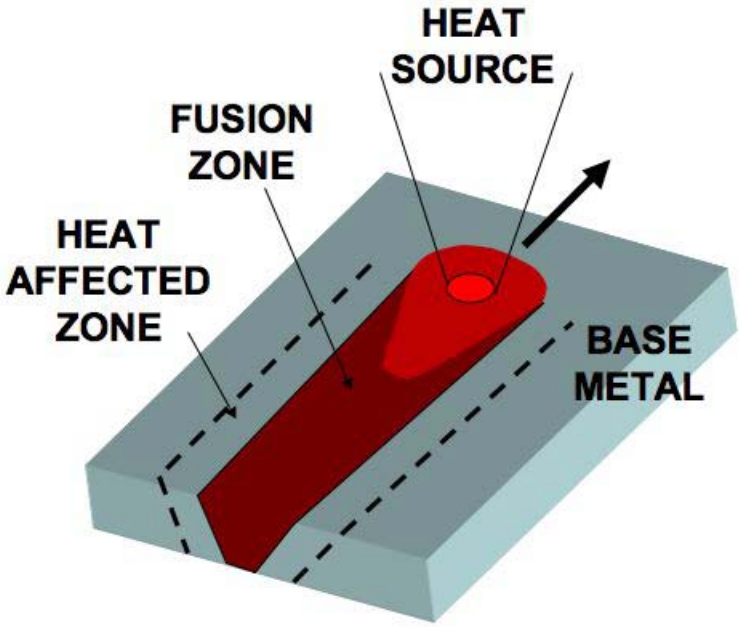

Fig. 13 Schematic of a fusion weld.

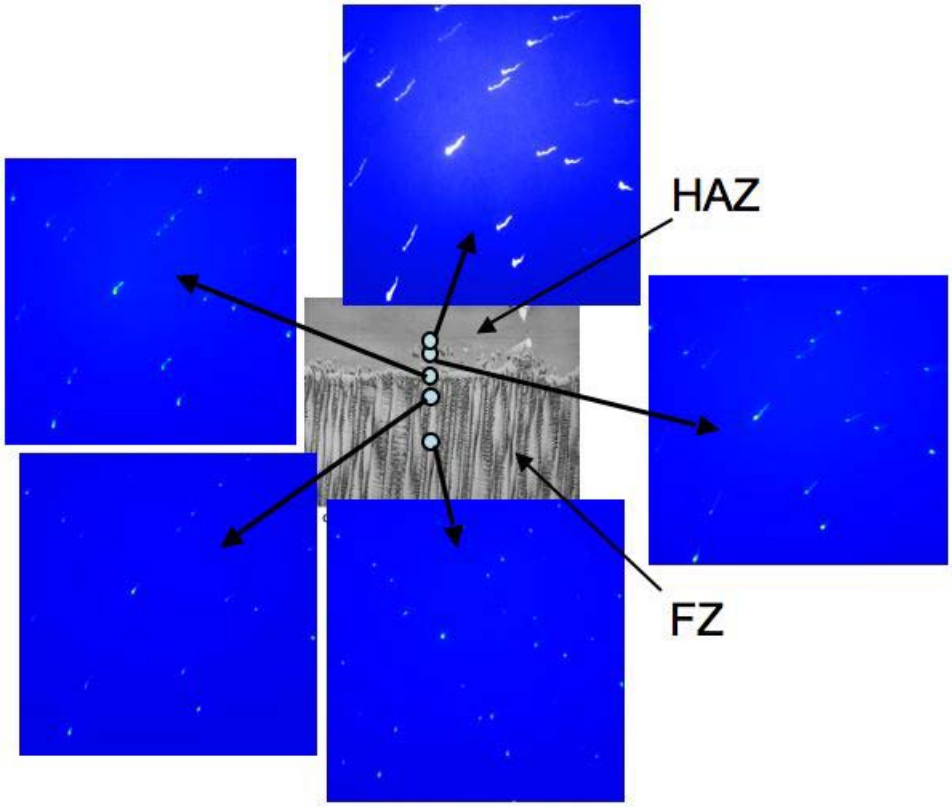

Fig. 14 Photomicrography of the fusion zone, with Laue mages from various parts of the weld matched to the weld region.